IEEE Access
Multidisciplinary : Rapid Review : Open Access Journal

Received March 27, 2022, accepted April 11, 2022, date of publication April 18, 2022, date of current version April 27, 2022.

Digital Object Identifier 10.1109/ACCESS.2022.3168350

A MEMS Fiber-Optic Fabry-Perot Vibration Sensor for High-Temperature Applications

JIANG QIAN[1], PINGGANG JIA[1,2], HUA LIU[1], QIANYU REN[1], JIA LIU[1], LI QIN[1], AND JIJUN XIONG[1]

[1]State Key Laboratory of Dynamic Measurement Technology, North University of China, Taiyuan 030051, China
[2]Key Laboratory for Micro/Nano Technology and System of Liaoning Province, Dalian University of Technology, Dalian 116081, China

Corresponding author: Pinggang Jia (pgjia@nuc.edu.cn)

This work was supported in part by the National Natural Science Foundation of China under Grant 52075505; in part by the Innovative Research Group Project of National Science Foundation of China under Grant 51821003; in part by the National Science and Technology Major Project of China under Grant J2019-V-0015-0110; and in part by the Open Project Program of Key Laboratory for Micro/Nano Technology and System of Liaoning Province of China, Dalian University of Technology.

ABSTRACT An extrinsic high-temperature fiber-optic Fabry-Perot vibration sensor based on MEMS technology is described and experimentally demonstrated. The sensitive unit consists of four cross beams with a central seismic mass batch-fabricated on a silicon wafer. The sensing head is fabricated by MEMS technology including dry etching, anodic bonding and dicing processing. And the optical fiber is intergrated in the sensing head by laser fusing. According to our calculation, the sensor has a resonance frequency of 10.008kHz. Experimental results indicated that the sensitivity of the sensor from 2g to 22g, with the frequency of 200Hz, was 2.48 nm/g at 20° and can work stably at 400°. The nonlinearity of the sensor was evaluated from 20° to 400° and the max nonlinear error was 1.88% at 300°. In addition, the temperature drift and temperature crossed sensitivity of the sensor agreed well with the theoretical analysis. We believe this proposed MEMS vibration sensor has a wide engineering high-temperature application prospect.

INDEX TERMS Fiber-optic, Fabry-Perot, high-temperature applications, MEMS, vibration measurement.

I. INTRODUCTION

High temperature vibration sensors are widely used in health monitor in aeroengine and gas turbine, wing of hypersonic vehicle, components or fuel cladding of nuclear reactor and automobile engines [1]–[6]. To date, there are many types of sensors developed for high temperature vibration applications such as piezoelectric sensors, piezoresistive sensors, capacitive sensors [7]–[11]. Compared with these traditional electrical sensors, fiber-optic sensors have the advantages of immunity to electromagnetic interference and optical interference is not influenced by temperature.

Different fabrication methods have been used to manufacture the sensing elements of fiber-optic sensors, including micro-machining, laser ablation, chemical etching, MEMS technology, etc. [12]–[16]. In the previous work, we proposed the two fiber-optic Fabry-Perot (F-P) accelerometers, of which the steel circular diaphragm and brass cantilever micromachined as the sensing elements, respectively [17]–[18]. However, due to the low machining resolution, the consistency of the sensor remained a large error. Li *et al.* [19] proposed an accelerometer with a micro-cantilever fabricated on one side of a single-mode optical fiber using ps-laser and focused ion beam. Zhao *et al.* [20] proposed a compact fiber-optic F-P accelerometer with metal mesh diaphragm-mass structure, achieving high-speed, high-resolution and real-time measurements. Zhang *et al.* [21] demonstrated an all-fiber sensor for low-frequency vibration measurements, in which the support beam and the mass was fabricated using chemical etching process. Chen *et al.* [12] proposed an in-line fiber optic F-P vibration sensor by fusing some hollow silica glass tubes and single-mode fiber which can work below 500°. The above processing methods cannot meet the requirement of batch fabrication. Edward *et al.* [16] reported a silicon MEMS F-P optical accelerometer, in which the displacement of the proof mass is mechanically amplified by a V-beam structure prior to transduction. Compared with machining, chemical etching processing and laser

The associate editor coordinating the review of this manuscript and approving it for publication was Sukhdev Roy.

This work is licensed under a Creative Commons Attribution 4.0 License. For more information, see https://creativecommons.org/licenses/by/4.0/

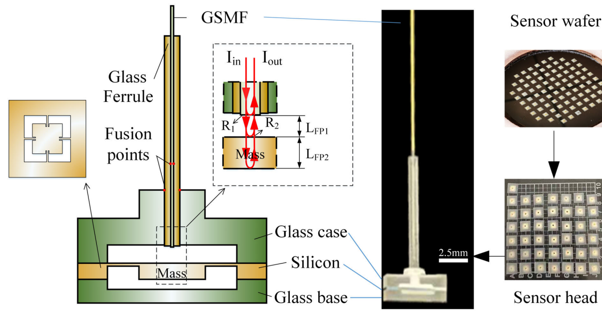

FIGURE 1. Schematic and photograph of the fiber-optic F-P vibration sensor.

processing, the sensor based on MEMS processing technology has the advantages of mass production, low cost and good consistency.

In this paper, we proposed a MEMS-based fiber-optic F-P vibration sensor. The sensors head was batch-fabricated on a silicon wafer and then separated by dicing processing. The end face of the fiber was laser-fused in parallel with the surface of the seismic mass. The temperature drift and temperature cross sensitivity of the sensor at high temperature were analyzed theoretically. A dual-wavelength demodulation system was used to demodulate the output of the sensor which was working at 20° to 400°. The experimental variation trends of the temperature drift and the temperature cross sensitivity are consistent with the theoretical calculation respectively. The proposed optical sensor is electromagnetic interference because of the sensing principle. And the output signal is transmitted through optical fiber in which way can solve the problem that conductor heat transfer affects the signal processing unit. Therefore, the sensor has the potential of applicable in higher temperature compared to conventional technology.

II. SENSOR WORKING PRINCIPLE AND FABRICATION

A. VIBRATION SENSING PRINCIPLE

Figure 1 shows the schematic and photograph of the fiber-optic F-P vibration sensor. The sensor consists of a gold-coated single mode fiber (GSMF), a glass ferrule, a glass case, a silicon cross beams with central seismic mass and a glass case. The sensing heads are batch-fabricated by anodically bonding the micromachined glass wafer and silicon wafer. The F-P cavity is constituted by fusing the end face of the GSMF in parallel with the surface of the seismic mass. The glass ferrule, the glass case and the glass wafer are Borofloat33 (BF33). The cross beams with central seismic mass is clamped by the glass case and the glass serving as a mass–spring–damper system to translating the inertial force of the seismic mass into the cavity length (LFP_1) change. When the on-axis acceleration is applied to the sensor, the displacement of the seismic mass included by the vibration causes the change of LFP_1, which is proportional to the phase shifts of the interference output.

According to Newton's second law and Euler-Bernoulli beam theory, when on-axis acceleration excitation is applied to the fiber-optic F-P vibration sensor, ignoring the lateral load of beams and the upper surface deformation of the seismic mass, the maximum deflection of the cross beam $\Delta\omega(t)$ (the on-axis displacement of the seismic mass) can be expressed as:

$$\Delta\omega(t) = -\frac{ml^3a(t)}{4Ebh^3} \tag{1}$$

where m is the mass of the seismic mass, a_{axi} is the on-axis acceleration, E is the Young's modulus of silicon, l, b, h are the length, width and height of the cross beam, respectively. The four cross beams have the same size. Therefore, the on-axis sensitivity of the sensor can be expressed as:

$$S = \frac{mgl^3}{4Ebh^3} \tag{2}$$

the acceleration we used is a gravitational acceleration so that the unit of the sensitivity is nm/g.

The resonance frequency of the mass-load cross beams can be given by:

$$f = \frac{1}{2\pi}\sqrt{\frac{4Ebh^3}{ml^3}} \tag{3}$$

According to Fig. 1, the L_{FP1} is sensitive to acceleration excitation. And the relationship between the phase shifts of the L_{FP1} ($\Delta\varphi(t)$) and the variation of the F-P cavity (L_{FP1}) length ($\Delta L(t)$) can be expressed as [22]:

$$\Delta\varphi(t) = \frac{4\pi n}{\lambda}\Delta L(t) \tag{4}$$

where n is the refractive index of air, λ is the wavelength of incident light. The variation of the length of the interference cavity ($\Delta L(t)$) caused by the on-axis acceleration excitation is numerically equal to the on-axis displacement of the seismic mass ($\Delta\varphi(t)$). Equations (1) and (4) then can be simplified into:

$$\Delta\varphi(t) = -\frac{mnl^3}{Ebh^3\lambda}\cdot a(t) \tag{5}$$

As shown in (4), when the wavelength of incident light λ is constant, $\Delta\varphi(t)$ and $a(t)$ are linearly proportional.

When the external temperature changes, the E, l, b, h in (2) will change due to the thermal expansion. According to the formulas that illuminate the relationship between thermal expansion coefficient of silicon and temperature ($\alpha(T)$) [23], and the relationship between Young's modulus of silicon and temperature ($E(T)$) [24], the sensitivity of the sensor at temperature T can be expressed as:

$$S(T) = \frac{m\cdot g\cdot l(T)^3}{4\cdot E(T)\cdot b(T)\cdot h(T)^3} \tag{6}$$

where the length (l), width (b), height (h) of the cross beam at temperature T can be expressed as:

$$\begin{bmatrix} l_{T_0} \\ b_{T_0} \\ h_{T_0} \end{bmatrix}\cdot(1+\alpha(T)\cdot(T-T_0)) = \begin{bmatrix} l(T) \\ b(T) \\ h(T) \end{bmatrix} \tag{7}$$

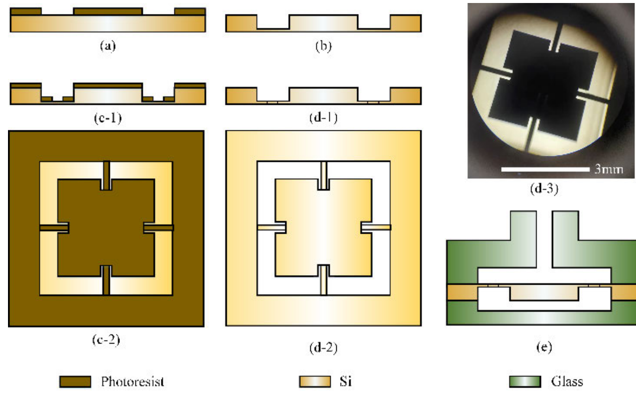

FIGURE 2. Fabrication process of the fiber-optic F-P vibration sensor based on the silicon wafer.

TABLE 1. Parameters of the fiber-optic F-P vibration sensor.

Symbol	Parameters	Units	Value
l	Length of beam	mm	0.9
b	Width of beam	mm	0.15
h	Thickness of beam	mm	0.06
ρ	Density of monocrystalline silicon	kg/m^3	2329
m_s	Mass of central seismic mass	gram	4.472×10^{-3}
E	Young's modulus of monocrystalline silicon	GPa	[24]
S	Sensitivity	nm/g	2.48
f_{res}	Resonance frequency	kHz	10.008
R	Resolution	mg	5.5

According to (1), the temperature drift of the L_{FP1} ($L_{dri}(T)$) mainly included by: bending of cantilever beam caused by temperature, which can result in on-axis displacement of the seismic mass; the on-axis thermal expansion of BF33 case; the on-axis thermal expansion of single mode fiber. The bending of cantilever beam caused by temperature is similar to the sensitivity difference at various temperatures in terms of the constant Young's modulus of silicon. The difference of sensitivity can be calculated by (6). The coefficient of BF33 case thermal expansion is a function of temperature [25]. The thermal expansion of single mode fiber is approximately equal to that of silica and varies little from 20° to 400°, which is about $5.5 \times 10^{-7}/K$. Thus, The temperature drift of the sensor $L_{dri}(T)$ can be approximately expressed as:

$$L_{dri}(T) = [S(T) - S(T_0)] + [L_{BF33}(T) - L_{BF33}(T_0)] - \left[L_f(T) - L_f(T_0)\right] \quad (8)$$

where $L_{BF33}(T)$ and $L_{BF33}(T_0)$ are the on-axis length of the BF33 case at T and T_0 respectively. $L_f(T)$ and $L_f(T_0)$ are the length of the single mode fiber at T and T_0 respectively. The length of the single mode fiber is equal to the distance from the fusion point to the end face of the fiber.

B. SENSOR FABRICATION

The sensor consists of a glass ferrule (BF33, I-boron Photoelectric Technology Co. Ltd. Wuhan. China), a single mode fiber (ASI9/125/155G, Fiberguide Industries, Ltd. New Jersey. USA), a glass case and a glass base (BF33/2.0T/4in, Jingshu Optoelectronic technology, Ltd. Suzhou. China), a monocrystalline silicon with cross beam (p, <110>).

The batch fabrication process mainly involves three steps. In the first step as shown in Figs. 2(a) - 2(b), with the help of the beforehand mask, the top surface of the silicon wafer was coated the photoresist with a thickness of approximately 10μm. The part covered by the center photoresist is the seismic mass area. Then the thickness reduction was operated to reach the 0.09mm of the cross beam through dry etching technology. After this, the photoresist layer was washed off in acetone solution. In step 2, as shown in Figs. 2(c-1) - 2(d-3), the shape of the cross beam was constructed in the thin area by the prior mask. Then, the suspended cross beam was constructed through dry etching technology, which was followed by dissolving the photoresist. Figs. 2(c-2) and (d-2) are the vertical views of (c-1) and (d-1), respectively. Fig. 2(d-3) is the photograph of the cross beam after etching. In step 3, as shown in Fig. 2(e), the glass substrate with 2mm thickness was mechanically drilled to form a through hole with the diameter of 1.0 mm and a groove with a depth of 200μm. The groove is square with the area of 5 × 5mm. In addition, a groove with a depth of 200μm was constructed on another glass with 1mm thickness by using the same method. Then, the silicon wafer was anodically bonded onto the two glass wafers. Next, the boss structure was then machined on the top of the glass with an outer diameter of 2 mm and a height of 1 mm. Finally, the wafer was split into separately units with a size of 7 mm × 7 mm. The detailed parameters of the F-P vibration sensor are listed in Table 1. According to Fig. 2(d-3), the structure designed in the paper increases the sensitivity of the structure to a certain extent by adding the mass of the inertial block under the condition that the size of the cantilever beam and the overall size remain unchanged. The lithography and etching are plane processing methods. The array structure is constructed on the four inches silicon wafer by using the mask. Once lithography and once etching can realize the processing of all sensitive elements in a single layer, so it has the characteristics of batch processing. However, the accuracy of the processing method used in this paper is affected not only by the quality of pretreatment manual processing like wafer cleaning, but also by mask accuracy and the precision of the machines and these effects are unavoidable.

Then, the GSMF with inner and outer diameters of 12μ and 1.0 mm, inserted into the glass ferrule. The ferrule protected the GSMF and avoided the vibration influence. The glass ferrule has an outer diameter of 1mm, an inner diameter of 0.126mm and a length of 16mm. The glass ferrule was inserted into the through hole, which was then fused with the substrate using a CO_2 laser fusion splicer (LZM-110, FUJIKURA). The laser power (bits) and fusion time (s) of

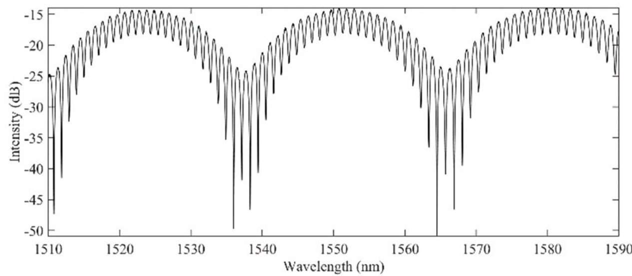

FIGURE 3. Spectrum of high temperature optical fiber vibration sensor.

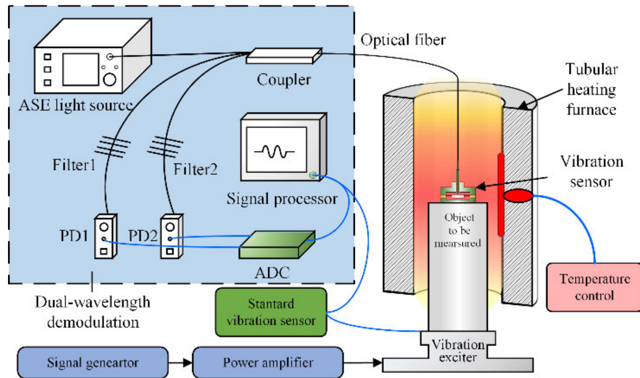

FIGURE 4. The experimental set up of the fiber-optic F-P vibration sensor for high-temperature test.

fusing GSMF and HST are 280 and 4, respectively. The laser power (bits) and fusion time (s) of fusing HST and the boss structure are 360 and 20, respectively. The designed parameters and performances of the proposed fiber-optic F-P sensor obtained by Equations. (2) and (3) are listed in Table 1. The spectrum of the processed fiber-optic F-P vibration sensor is shown in Fig. 3. The fiber-optic FP sensor with low interference fineness can be approximated as double beam interference, and the influence of multi-beam interference is very small and can be ignored. In this paper, the dual wavelength demodulation technology [26] was used to interrogate the change of the change of the cavity length of the shortest F-P cavity (L_{FP1}).

III. EXPERIMENTAL RESULTS AND DISCUSSIONS

The experimental setup was built to characterize the fiber-optic F-P vibration sensor at a high temperature environment, as shown in Fig. 4. It consisted of a vibration excitation system, a tubular heating furnace, a standard vibration sensor and a dual wavelength demodulation system. The fiber-optic F-P vibration sensor was on a metal rod with a high-temperature glue (YK–8927, Yikun glue, Macheng, China), and together put into the tubular heating furnace (GSL-1100 X-S, HF kejing, Hefei, China). The metal rod was connected to the vibration exciter (TV 50101, Tira, Thuringen, Germany). The light derived from the ASE light source reached the fiber-optic F-P vibration sensor through the single mode fiber and the 3dB optical fiber coupler. According to Fig. 1 and Fig.3, the sensor is a multi-cavity F- P interferometer consisted of LFP_1 (39.74μm) and LFP_2 (300μm). The coupler splits the beam into two paths that passed through two optical fiber broadband filters with center wavelengths of 1548.14 nm and 1552.744 nm. The length of LFP_1 is shorter than LFP_2. The demodulation technology in Fig. 4, using an ASE light source and two optical fiber broadband filters, the interference only occurs in a shortest FP cavity that is shorter than the half of the coherence length. The bandwidth of both filters was 15 nm. Two interferometric signals at each center wavelength were obtained using two photodiodes (PDs), PD1 and PD2 (New Focus, 2503-FC-M). The detectable wavelength the PDs ranges from 900 to 1700nm. The voltage signals were collected by analog-to-digital conversion (ADC) and transmitted to a signal processor. The demodulation speed was 500 kHz.

The fiber-optic F-P vibration sensor was evaluated under temperatures ranging from 20°C to 400°C, with an incrementof 100°C. At each temperature step, the sensor was tested from approximately 2g to 22g, with an increment of 2g. The excitation frequency was 200Hz. When loading the vibration, the accelerations was kept constant for 1 min at each point to record the vibration output accurately. Fig 5 (a) and (c) shown the vibration waveform of the sensor at 20°C and 400°C, respectively. According to the peak–peak phase value, the phase sensitivity of the system can reach to 0.04 rad/g (20°C) and 0.057rad/g (400°C), respectively. Fig. 5(b) and (d) are the fast Fourier transforms calculated by MTALAB corresponding to the waveforms Fig. 5(a) and (c). According to Figs. 5(b) and (d), the frequency of the vibration excitation is 200Hz, and the higher modes at 400Hz, 600Hz, 800Hz, etc. result from the deviation of the demodulation system instead of the higher modes of the vibration in the sensor. The phase difference of the dual-wavelength demodulation technology changes when the cavity length changes. It deviates from the orthogonal state to some extent. This will increase the error of the demodulation system and affect the accuracy of the demodulation system.

Actually, the temperature variation could introduce the phase change of sensor. However, compared with vibration, the frequency of phase changing caused by temperature variation is relatively lower. And then we performed high pass filtering on the output of the sensor in order to obtain the output caused by vibration. The output about vibration in Figs. 5, 6(b), 7 were obtained after high pass filtering.

According to Equation (5), the direct-current (DC) output phase of the vibration waveform at each temperature was the temperature drift of the fiber-optic F-P vibration sensor. The DC output phase of the sensor at 20°C was regarded as the reference of the temperature drift. Fig. 6(a) showed the temperature drift of the fiber-optic F-P vibration sensor. The black dots in the Fig. 6(a) were the measured value of temperature drift of the sensor. The red dotted line was the theoretical value followed Equation (9). The two values are in the same order of magnitude and show the same trend in the change of temperature. Fig. 6(b) illustrated the sensitivity of the

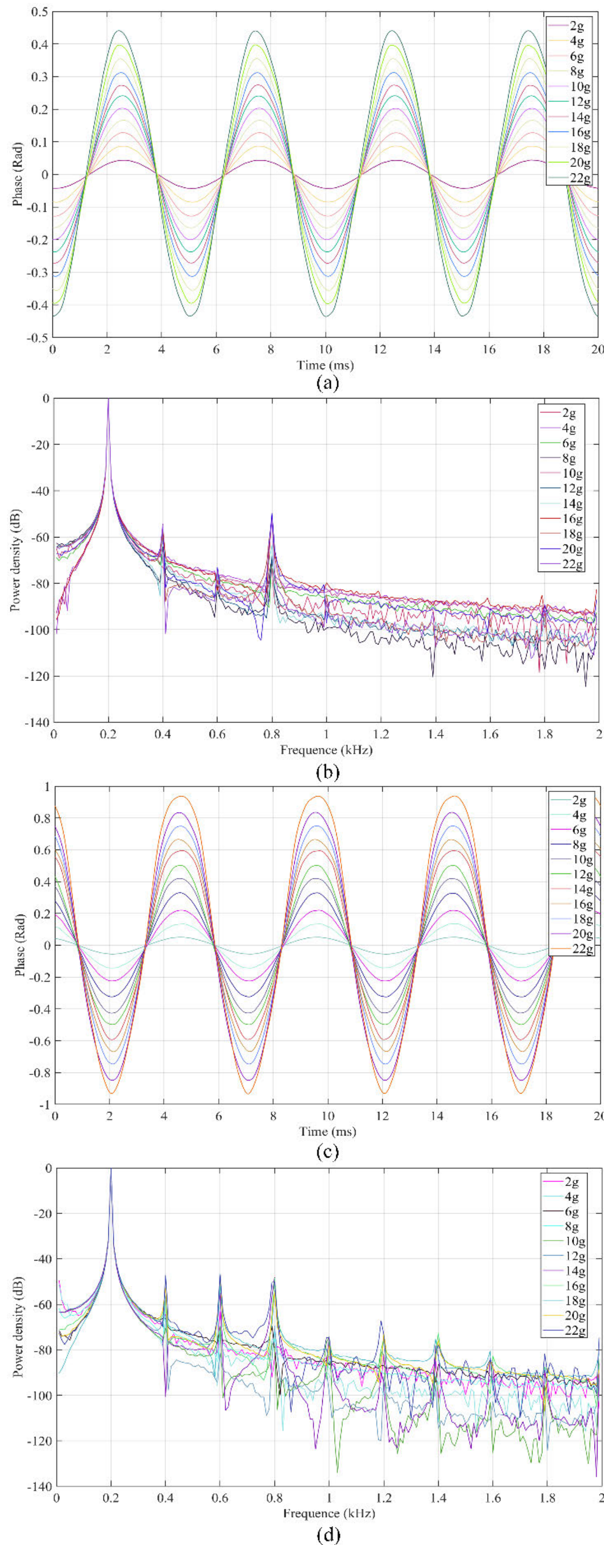

FIGURE 5. Output of the sensor from 2 g to 22 g under 200 Hz at 20°C and 400°C (a) Waveform of the sensor at 20°C (b) the fast Fourier transform of the waveform at 20°C (c) Waveform of the sensor at 400°C (d) the fast Fourier transform of the waveform at 400°C.

vibration object and the vibration sensor from 20°C to 400°C, respectively. The red dotted line was the measured value of the vibration object. The black dots were the theoretical value in Equations (7) and (8). The two values has the same trend with the change of temperature. Due to the residual stress generated by the sensor during processing and the machining error lead to the deviation between the experimental results and the model used to predict the theoretical value.

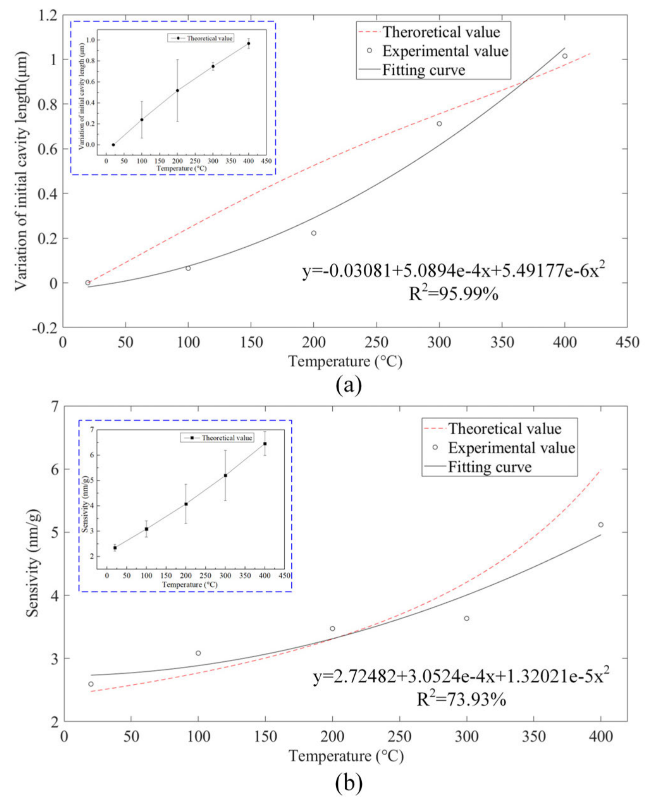

FIGURE 6. Temperature characteristics of the fiber-optic F-P vibration sensor and the error bar of the theoretical value with the experimental value (a) The temperature drift of the sensor (b) The temperature cross sensitivity of the sensor.

The fiber-optic F-P vibration sensor was evaluated under temperatures ranging from 20° to 400°. We record the peak-peak output of the sensor under each temperature and they were linear fitted by MATLAB. Fig. 7(a) shows that the slope of the fitted line were elevated with the temperature increasing. This is caused that the elastic modulus of silicon decreases with the increase of temperature. The slopes in Fig. 7(a) are the sensitivity in Fig. 6(b). Fig. 7(b) shows the error bar of the difference between the output of the sensor and the linear fitting value. According to the definition, under each temperature, the maximum error between the data we recorded and the new data we linear fitted divided the range of the sensor in order to obtain the max nonlinear errors.

The fiber-optic F-P vibration sensor was evaluated under frequency ranging from 100Hz to 2000Hz, with the increment of 100Hz, at 20°. The output phase of the sensor shown in Fig. 8(a) have no obvious change in the range of 100Hz - 2000Hz, which indicated that the frequency range of the vibration was much smaller than the resonance

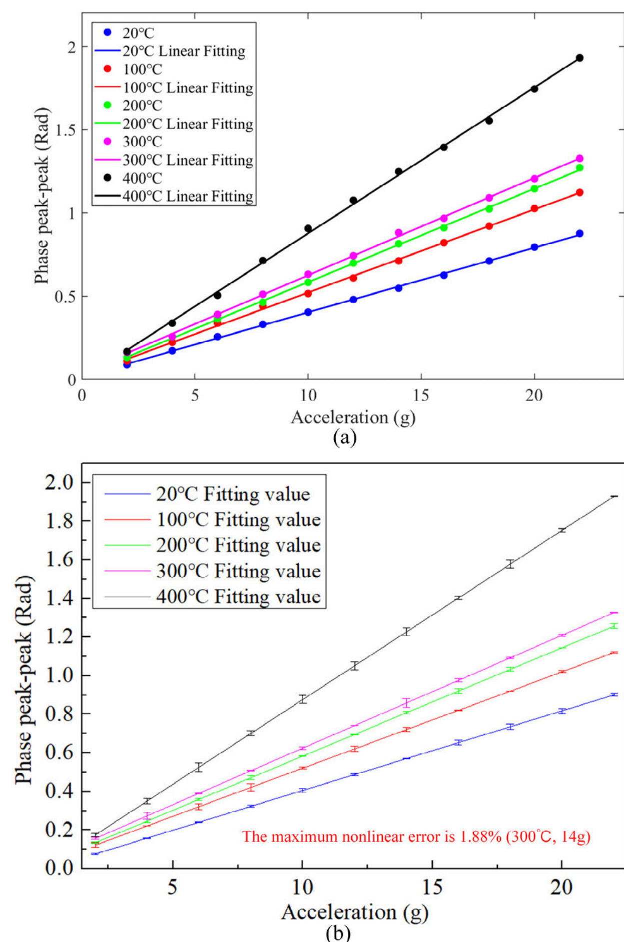

FIGURE 7. Linearity and nonlinear error of the fiber-optic F-P vibration sensor (a) Phase peak-peak of the sensor at different temperatures (b) the error bar of the fitting value with the experimental value and the maximum nonlinear error of the sensor.

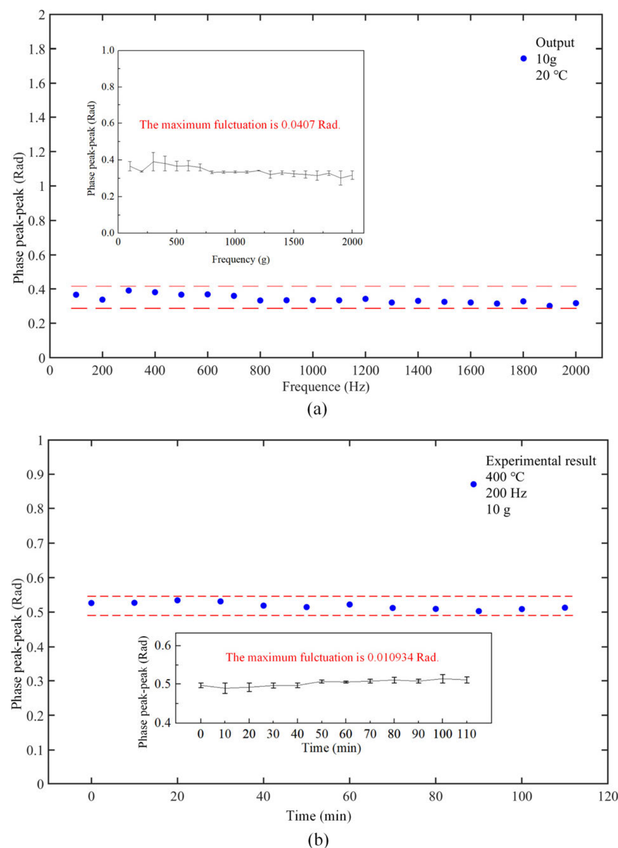

FIGURE 8. (a) Relationship between phase and frequency. (b) Stability of the fiber-optic F-P vibration sensor.

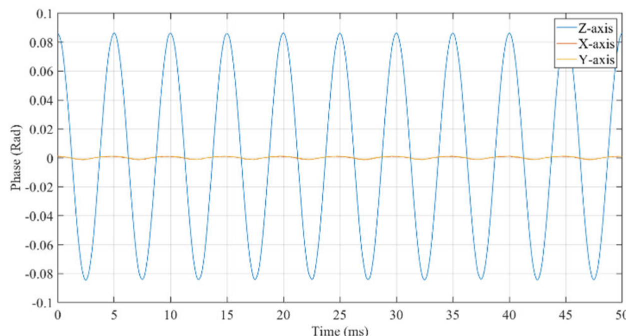

FIGURE 9. The axial and radial vibration response of the sensor.

frequency of the sensor. This was consistent with the resonance frequency calculated theoretically in Table 1. We averaged the output of the sensor and subtracted the average value from the output of the sensor to obtain the error bar shown in Fig. 8(a). And the maximum fluctuation is 0.0407 rad. In terms of the stability of the sensor, according to Fig. 8(b), we set the temperature, frequency and acceleration as 400°, 200Hz and 10g, respectively. We also averaged the output of the sensor and subtracted the average value from the output of the sensor within 110minutes to obtain the error bar. The maximum fluctuation is 0.010934 rad.

In order to determine the relationship between the axial vibration and the radial vibration, the sensor was respectively installed in 3 directions (X-axis, Y-axis, Z-axis). The Z-axis is the axial direction and the other directions are the axial radial directions of the sensor. We respectively recorded the outputs of the 3 directions when we applied 4g acceleration at a frequency of 200Hz. The outputs of the sensor in 3 directions is shown in Fig. 9. When the sensor was operated in Z-axis, X-axis and Y-axis, the phase peak-peak were 0.08638 rad, 0.001173 rad, 0.001052 rad, respectively. And the sensitivities of the sensor operated in Z-axis, X-axis and Y-axis are shown in Table 2. It can be seen that the sensitivity of the X-axial vibration is 73.64 times that of the radial vibration.

TABLE 2. Sensitivities of the sensor operated in 3 directions.

Direction	Sensitivity
X	0.00092325rad/g
Y	0.000263rad/g
Z	0.021595rad/g

TABLE 3. Comparison of proposed FP vibration sensors by different fabrication methods.

Fabrication method	Resonance Frequency (Hz)	Sensitivity	Maximum tested temperature
Micro-machining	393	11.3rad/g	80 °C [17]
Laser ablation	1560	100.807nm/g	Room temperature [19]
Chemical etching	107-178	0.35V/g	120°C [21]
MEMS	11750	0.081rad/g	Room temperature [16]
This work (MEMS)	**10008**	**2.48nm/g (0.08638rad/g)**	**400 °C**

The sensitivity of the Y-axial vibration is 82.11 times that of the radial vibration. Because the excitation unit is not completely horizontal, the output of the sensor at radial direction may be lower than the value we recorded. As listed in Table 3., the proposed FP vibration sensor fabricated by MEMS can be used to measure vibration at 400°.

IV. CONCLUSION

In this paper, a fiber-optic F-P vibration sensor for high-temperature applications based on MEMS technology was designed and experimentally demonstrated. The sensor head had high consistency and can be batch-fabricated. The characterization of the vibration sensor including resonance frequency, temperature drift and temperature crossed sensitivity at different temperature can be evaluated in theory. Owning to these characteristics, the proposed sensor has a wide engineering high-temperature application prospect.

REFERENCES

[1] D. Wu, L. Lin, and H. Ren, "Thermal/vibration joint experimental investigation on lightweight ceramic insulating material for hypersonic vehicles in extremely high-temperature environment up to 1500 °C," *Ceram. Int.*, vol. 46, no. 10, pp. 14439–14447, Jul. 2020.
[2] M. Khalid and P. David, "A review of hybrid fiber-optic distributed simultaneous vibration and temperature sensing technology and its geophysical applications," *Sensors*, vol. 17, no. 11, pp. 2511–2535, Nov. 2021.
[3] G. Gregori, L. Lì, J. A. Nychka, and D. R. Clarke, "Vibration damping of superalloys and thermal barrier coatings at high-temperatures," *Mater. Sci. Eng., A*, vol. 466, nos. 1–2, pp. 256–264, Sep. 2007.
[4] E. Rokicki, R. Przysowa, J. Kotkowski, and P. Majewski, "High temperature magnetic sensors for the hot section of aeroengines," *Aerospace*, vol. 8, no. 9, p. 261, Sep. 2021, doi: 10.3390/aerospace8090261.
[5] H. Kim, S. Kerrigan, M. Bourham, and X. Jiang, "AlN single crystal accelerometer for nuclear power plants," *IEEE Trans. Ind. Electron.*, vol. 68, no. 6, pp. 5346–5354, Jun. 2021.
[6] R. W. Johnson, J. L. Evans, P. Jacobsen, J. R. R. Thompson, and M. Christopher, "The changing automotive environment: High-temperature electronics," *IEEE Trans. Electron. Packag. Manuf.*, vol. 27, no. 3, pp. 164–176, Jul. 2004.
[7] K. Kim, S. Zhang, W. Huang, F. Yu, and X. Jiang, "$YCa_4O(BO_3)_3$ (YCOB) high temperature vibration sensor," *J. Appl. Phys.*, vol. 109, no. 12, Jun. 2011, Art. no. 126103.
[8] C. Jiang, X. Liu, F. Yu, S. Zhang, H. Fang, X. Cheng, and X. Zhao, "High-temperature vibration sensor based on Ba2TiSi2O8 piezoelectric crystal with ultra-stable sensing performance up to 650 °C," *IEEE Trans. Ind. Electron.*, vol. 68, no. 12, pp. 12850–12859, Dec. 2021.
[9] X. Jiang, K. Kim, S. Zhang, J. Johnson, and G. Salazar, "High-temperature piezoelectric sensing," *Sensors*, vol. 14, no. 1, pp. 144–169, 2014.
[10] D. J. Young, J. Du, C. A. Zorman, and W. H. Ko, "High-temperature single-crystal 3C-SiC capacitive pressure sensor," *IEEE Sensors J.*, vol. 4, no. 4, pp. 464–470, Jul. 2004.
[11] E. J. Eklund and A. M. Shkel, "Single-mask fabrication of high-G piezoresistive accelerometers with extended temperature range," *J. Micromech. Microeng.*, vol. 17, no. 4, pp. 730–736, Apr. 2007.
[12] R. Lv, Y. Zhao, and Q. Wang, "An optical fiber temperature sensor based on an ethanol filled Fabry–Perot cavity," *Instrum. Sci. Technol.*, vol. 42, no. 4, pp. 402–411, Jul. 2014.
[13] Z. Wang, W. Zhang, J. Han, W. Huang, and F. Li, "Diaphragm-based fiber optic Fabry–Perot accelerometer with high consistency," *J. Lightw. Technol.*, vol. 32, no. 24, pp. 4208–4213, Dec. 1, 2014.
[14] L. Zhang, Y. Jiang, J. Jia, P. Wang, S. Wang, and L. Jiang, "Fiber-optic micro vibration sensors fabricated by a femtosecond laser," *Opt. Lasers Eng.*, vol. 110, pp. 207–210, Nov. 2018.
[15] M. D. Pocha, G. A. Meyer, C. F. McConaghy, S. P. Swierkowski, and J. D. Wolfe, "Miniature accelerometer and multichannel signal processor for fiber optic Fabry–Perot sensing," *IEEE Sensors J.*, vol. 7, no. 2, pp. 285–292, Feb. 2007.
[16] E. Davies, D. S. George, and A. S. Holmes, "Mechanically amplified MEMS optical accelerometer with FPI readout," *Proc. SPIE*, vol. 8977, Mar. 2014, Art. no. 89770Z.
[17] D.-H. Wang and P.-G. Jia, "Fiber optic extrinsic Fabry–Perot accelerometer using laser emission frequency modulated phase generated carrier demodulation scheme," *Opt. Eng.*, vol. 52, no. 5, May 2013, Art. no. 055004.
[18] P.-G. Jia, D.-H. Wang, G. Yuan, and X.-Y. Jiang, "An active temperature compensated fiber-optic Fabry–Perot accelerometer system for simultaneous measurement of vibration and temperature," *IEEE Sensors J.*, vol. 13, no. 6, pp. 2334–2340, Jun. 2013.
[19] J. Li, G. Y. Wang, J. N. Sun, R. R. J. Maier, W. N. Macpherson, D. P. Hand, and F. Z. Dong, "Micro-machined optical fiber side-cantilevers for acceleration measurement," *IEEE Photon. Technol. Lett.*, vol. 29, no. 21, pp. 1836–1839, Nov. 1, 2017.
[20] Z. Zhao, Z. Yu, K. Chen, and Q. Yu, "A fiber-optic Fabry–Perot accelerometer based on high-speed white light interferometry demodulation," *J. Lightw. Technol.*, vol. 36, no. 9, pp. 1562–1567, May 1, 2018.
[21] Q. Zhang, T. Zhu, Y. S. Hou, and K. S. Chiang, "All-fiber vibration sensor based on a Fabry–Perot interferometer and a microstructure beam," *J. Opt. Soc. Amer. B, Opt. Phys., Opt. Phys.*, vol. 30, no. 5, pp. 1211–1215, May 2013.
[22] X. Wang, S. Wang, J. F. Jiang, K. Liu, P. Zhang, W. Wu, and T. G. Liu, "High-accuracy hybrid fiber-optic Fabry–Perot sensor based on MEMS for simultaneous gas refractive-index and temperature sensing," *Opt. Exp.*, vol. 27, no. 4, pp. 4204–4215, 2019.
[23] Y. Okada and Y. Tokumaru, "Precise determination of lattice parameter and thermal expansion coefficient of silicon between 300 and 1500 K," *J. Appl. Phys.*, vol. 56, no. 2, pp. 314–320, Jul. 1984.
[24] R. Melamud, S. A. Chandorkar, K. Bongsang, L. Hyung Kyu, J. C. Salvia, G. Bahl, M. A. Hopcroft, and T. W. Kenny, "Temperature-insensitive composite micromechanical resonators," *J. Microelectromech. Syst.*, vol. 18, no. 6, pp. 1409–1419, Dec. 2009.
[25] L. S. Sinev and I. D. Petrov, "Linear thermal expansion coefficient (at temperatures from 130 to 800 K) of borosilicate glasses suitable for silicon compounds in microelectronics," *Glass Ceram.*, vol. 73, nos. 1–2, pp. 32–35, May 2016.
[26] Q. Y. Ren, P. G. Jia, G. W. An, J. Liu, G. C. Fang, W. Y. Liu, and J. J. Xiong, "Dual-wavelength demodulation technique for interrogating a shortest cavity in multi-cavity fiber-optic Fabry–Perot sensors," *Opt. Exp.*, vol. 29, no. 20, pp. 32658–32669, Sep. 2021.

JIANG QIAN received the B.Sc. degree in microelectronics from the North University of China, China, in 2016, where he is currently pursuing the Ph.D. degree. His research interests include fiber optic vibration sensors, MEMS, and high temperature sensors.

PINGGANG JIA received the Ph.D. degree in instrument science and technology from Chongqing University, Chongqing, China, in 2013. He is currently a Professor with the North University of China, where he is also a Staff of the Micro and Nano Technology Research Center. His research interests include fiber optic sensors, MEMS, laser-based measurement technology, and high-temperature.

HUA LIU received the B.Sc. degree in electronic science and technology from the North University of China, China, in 2020, where she is currently pursuing the master's degree. Her research interests include fiber optic vibration sensors, MEMS, and high temperature sensors.

QIANYU REN received the B.S. and M.S. degrees from the North University of China, Shanxi, China, in 2014 and 2018, respectively, where he is currently pursuing the Ph.D. degree. His current research interests include fiber sensing and demodulation technology.

JIA LIU received the B.Sc. and Ph.D. degrees from the North University of China, Shanxi, China, in 2014 and 2020, respectively. She is currently a Lecturer with the North University of China. Her current research interests include the high temperature sensors and MEMS devices.

LI QIN received the Ph.D. degree in instrument science and technology from the North University of China, Shanxi, China, in 2006. She is currently a Professor with the North University of China, where she is also a Doctoral Supervisor. Her research interests include integrated measurement system and instruments, micro inertial measurement systems, dynamic test, and reliability analysis.

JIJUN XIONG received the B.S. and M.S. degrees in electrical engineering from the North University of China, Shanxi, China, in 1993 and 1998, respectively, and the Ph.D. degree in precision instruments and technology from Tsinghua University, Beijing, China, in 2003. He is currently a Professor with the North University of China. His research interests include dynamic testing technology and micro nano sensors and systems.